Mitochondrial DNA Damage in Iron Overload

Xueshan Gao, Jian Li Campian, Mingwei Qian, Xiao-Feng Sun and John Wallace Eaton

Original Publication:

Xueshan Gao, Jian Li Campian, Mingwei Qian, Xiao-Feng Sun and John Wallace Eaton, Mitochondrial DNA Damage in Iron Overload, 2009, JOURNAL OF BIOLOGICAL CHEMISTRY, (284), 8, 4767-4775.
http://dx.doi.org/10.1074/jbc.M806235200

Mitochondrial DNA Damage in Iron Overload

Xueshan Gao[1,2], Jian Li Campian[1], Mingwei Qian[1], Xiao-Feng Sun[1], and John W. Eaton[1,2,3]

1 Department of Oncology, University of Linköping, Linköping, Sweden
2 Molecular Targets, J. G. Brown Cancer Center
3 Department of Pharmacology and Toxicology, University of Louisville, Louisville, Kentucky

Abstract

Chronic iron overload has slow and insidious effects on heart, liver, and other organs. Because iron-driven oxidation of most biologic materials (such as lipids and proteins) is readily repaired, this slow progression of organ damage implies some kind of biological "memory." We hypothesized that cumulative iron-catalyzed oxidant damage to mtDNA might occur in iron overload, perhaps explaining the often lethal cardiac dysfunction. Real time PCR was used to examine the "intactness" of mttDNA in cultured H9c2 rat cardiac myocytes. After 3–5 days exposure to high iron, these cells exhibited damage to mtDNA reflected by diminished amounts of near full-length 15.9-kb PCR product with no change in the amounts of a 16.1-kb product from a nuclear gene. With the loss of intact mtDNA, cellular respiration declined and mRNAs for three electron transport chain subunits and 16 S rRNA encoded by mtDNA decreased, whereas no decrements were found in four subunits encoded by nuclear DNA. To examine the importance of the interactions of iron with metabolically generated reactive oxygen species, we compared the toxic effects of iron in wild-type and rho^{o} cells. In wild-type cells, elevated iron caused increased production of reactive oxygen species, cytostasis, and cell death, whereas the rho^{o} cells were unaffected. We conclude that long-term damage to cells and organs in iron-overload disorders involves interactions between iron and mitochondrial reactive oxygen species resulting in cumulative damage to mtDNA, impaired synthesis of respiratory chain subunits, and respiratory dysfunction.

Introduction

Patients with primary or secondary iron overload are liable to cardiac and hepatic failure, and type II diabetes. Iron is required for the activity of numerous iron- and heme-containing proteins, but "free" (*i.e.* redox active) iron catalyzes the formation of highly toxic reactive oxygen species (ROS) (2) that damage lipids, proteins, and DNA (1). This damage is assumed to arise from iron-catalyzed hydroxyl radical formation or, perhaps more likely, iron-centered radicals such as ferryl and perferryl (2, 3). Iron-driven oxidation events require that the metal interact with cellular oxidizing and reducing equivalents such as superoxide and hydrogen peroxide, a major source of which is "leak" of electrons from the mitochondrial electron transport chain (4–6).

The present investigations were focused on the etiology of iron-mediated cardiac damage and specifically on the question of why, in patients with chronic iron overload, damage to organs

such as the heart develops over a period of years, whereas most types of iron-mediated oxidation events can be repaired within minutes or hours. We have investigated the hypothesis that cumulative damage to DNA, specifically mtDNA, is critical to the slow development of cardiac dysfunction in chronic iron overload. In partial support of this idea, earlier studies clearly show that iron does promote DNA base oxidation as well as single and double strand DNA breaks. Mitochondrial DNA may be particularly vulnerable to such oxidation events inasmuch as it lacks histones, has less effective repair systems and, perhaps most importantly, resides within an organelle that ceaselessly generates ROS.

Here, we report that, in cultured rat cardiac myocytes, iron overload causes (i) progressive loss of intact mtDNA, (ii) decreased expression of respiratory chain subunits encoded by mitochondrial, but not nuclear, DNA, and (iii) diminished respiratory function. Furthermore, it appears that iron-mediated cytotoxicity involves ROS generated by the mitochondrion itself because cells lacking mtDNA (and, therefore, respiration) are remarkably tolerant of iron overload. Overall, our results suggest that the slowly developing cardiac dysfunction seen in chronic iron overload arises secondary to cumulative iron-driven oxidant damage to mtDNA.

Experimental Procedures

Cells and Reagents—Rat cardiac myocyte H9c2 cells were obtained from the American Type Culture Collection (Rockville, MD). Dulbecco's modified Eagle's medium (DMEM), phosphate-buffered saline (PBS), trypsin-EDTA, annexin V-fluorescein isothiocyanate, agarose powder, and fetal bovine serum were obtained from Invitrogen. Hydroxyethyl starch: desferrioxamine conjugate (M_r > 200,000) was kindly provided by Biomedical Frontiers, Inc. (Minneapolis, MN). Pico Green, JC-1, and dichlorofluorescein diacetate were obtained from Molecular Probes (Eugene, OR). Perchloric acid was purchased from Fisher Scientific (Pittsburgh, PA). Hanks' balanced salt solution (HBSS), ethidium bromide, Ferene S (3-(2-pyridyl)-5,6-di(2-furyl)-1,2,4-triazine-5',5'-disulfonic acid), ferric ammonium citrate (FAC), L-ascorbic acid (sodium salt), bovine heart cytochrome *c*, chloramphenicol, sodium citrate, potassium phosphate, ethyl acetate, guanidine, porcine heart isocitrate dehydrogenase, sodium citrate, NADH, $MnCl_2$, 2,4-dinitrophenyl hydrazine, sucrose, potassium phosphate, EDTA, Tris, ethyl acetate, bovine serum albumin (BSA), 5,5'-dithiobis(2-nitrobenzoic acid), carbonyl cyanide *m*-chlorophenylhydrazone (CCCP), Chelex 100, and Tween 80 were purchased from Sigma Co.

Cell Culture—H9c2 cells were cultured in DMEM supplemented with 10% heat-inactivated fetal bovine serum at 37 °C in a humidified atmosphere of 5% CO_2 and 95% air. Stock cultures were grown in polystyrene T-75 culture flasks in a Forma Scientific incubator. The cells were split 1:10 every 3–4 days. For experiments involving exposure to iron (in the form of FAC), cells were initially plated at varying densities because we found that the toxic effects of added FAC were highly dependent on cell density (with more dense cultures being more resistant to iron toxicity). Therefore, for experiments involving longer term exposure to higher

iron concentrations (*e.g.* results shown in Figs. 1-4, 7-9) cell cultures were 60% confluent upon the addition of FAC, whereas for studies of toxicity under growth conditions

(Figs. 5 and 6) cultures were 10% confluent at the start. For determinations of cell growth rate, cells were seeded in 48-well semi-microtiter plates (2 x 10^4 cells/well) for 24 h prior to the addition of FAC. Cell numbers were verified by hemocytometer counts of trypan blue excluding cells detached with trypsin/EDTA.

Cell Viability Assay—Cell viability was estimated by measurements of Alamar blue reduction (7). Wild-type H9c2 and rho^o H9c2 cells were grow on 48-well semi-microtiter plates as above and exposed to iron. Following iron exposure, Alamar Blue reduction was measured, fluorescence of the reduced dye being read at 530 nm excitation and 590 nm emission using a spectrofluorometric plate reader (Molecular Devices Corp., Sunnyvale, CA).

Intracellular Iron Assays—For histochemical analyses of intracellular iron using calcein staining, H9c2 cells were seeded in 48-well plates (5000 cells/well). After 24 h, the cells were exposed to 200 μM FAC for 24 h. Following this, the cells were rinsed with HBSS (containing Ca^{2+} and Mg^{2+}) and stained with calcein AM (final concentration: 5 μM diluted in complete HBSS) for 30 min. The cells were then rinsed with HBSS buffer and calcein fluorescence was evaluated using fluorescence microscopy.

The accumulation of iron within test cells was also measured colorimetrically as previously described (8). Briefly, the cells were grown in 100-mm plates under normal culture conditions. Following exposure to iron, the cells were detached with trypsin/EDTA containing 1 mM desferrioxamine equivalents of the high molecular weight hydroxyethyl starch:desferrioxamine conjugate to remove any extracellular iron. The cells then were washed in ice-cold Chelex-treated PBS three times. For iron measurements, a 300-μl suspension containing 3 x 10^6 cells was extracted with 200 μl of ice-cold 25% perchloric acid (final concentration = 10%). Following 30 min incubation on ice, the precipitate was centrifuged at 12,000 x *g* for 5 min and 400 μl of supernatant was used for assay of "loose" iron. Assays contained 400 μl of the supernatant, 100 μl of freshly prepared 0.25 M sodium ascorbate, 400 μl of 40% (w/v) ammonium acetate, and 100 μl of 3.0 mg/ml Ferene S. Absorbance was measured at 594 nm and the results were calculated using an extinction coefficient of 35.5 mM^{-1} cm^{-1} for the Ferene S:iron chelate (9, 10). For measurements of total residual iron, the precipitate was digested with 100 μl of 50% nitric acid at 56 °C for 24 h. Following the addition of NaOH to neutralize the nitric acid, iron was assayed as described above.

Determination of Protein Carbonyls—Cell lysates and mitochondria were prepared from cell suspensions washed twice with cold mitochondrial isolation buffer (250 mM sucrose, 10 mM Tris-HCl, 1 mM desferrioxamine equivalents of high molecular weight hydroxyethyl starch:desferrioxamine conjugate, 1 mM EDTA, pH 7.8). The cells were suspended in this isolation buffer to 8 x 10^6 cells/ml and disrupted by nitrogen cavitation at 4 °C using an ice-

cooled cell disruption bomb (Parr Instrument Co., Moline, IL). Total cell lysates were used directly for carbonyl assays and mitochondria were prepared by differential centrifugation using a modification of the procedure described by Fuller *et al.* (11). Following removal of large debris by centrifugation at 500 x *g* for 10 min at 4 °C, the supernatants were centrifuged at 14,000 x *g* for 20 min at 4 °C to obtain mitochondrial pellets. The total protein carbonyl content of whole cell lysates and mitochondria was determined by reaction with 2,4-dinitrophenyl hydrazine using a slight modification of the method of Levine *et al.* (12).

Samples containing 300 µg of protein were incubated with 500 µl of 10 mM 2,4-dinitrophenyl hydrazine in 2 M HCl at room temperature for 1 h with intermittent mixing. Following the addition of 500 µl of 20% (w/v) ice-cold trichloroacetic acid, the samples were centrifuged at 11,000 x *g* for 3 min. The supernatant was discarded and the pellets were washed three times with 1 ml of ethanol:ethyl acetate (1:1) to remove unreacted 2,4-dinitrophenyl hydrazine. The protein pellet was redissolved in 0.6 ml of 6 M guanidine with 20 mM K_2HPO_4 (pH adjusted to 2.3 with 20% trichloroacetic acid) and any insoluble material was removed by centrifugation at 11,000 x *g* for 3 min. The carbonyl content in the supernatant was measured spectrophotometrically at 375 nm. Results were calculated using an absorbance coefficient of 22,000 M^{-1} cm^{-1} and normalized for protein concentration measured using a bichinchoninc acid reaction (Pierce).

Total Cellular DNA Isolation—Total DNA was isolated using the QIAamp DNA isolation kit (Qiagen, Valencia, CA) according to the manufacturer's protocol. Briefly, following exposure to varying concentrations of iron, the cells were detached with trypsin/EDTA containing 1 mM desferrioxamine equivalents of the high molecular weight hydroxyethyl starch:desferrioxamine conjugate to remove adventitious iron. The cells then were washed in ice-cold Chelex-treated PBS three times. The cells were counted using a hemocytometer (Fisher Scientific, Pittsburgh, PA) prior to DNA isolation. DNA was quantified using PicoGreen® (Molecular Probes, Eugene, OR) with fluorescence measured at 485 nm excitation and 525 nm emission using a spectrofluorometric plate reader (Molecular Devices Corp., Sunnyvale, CA).

PCR Amplification—To assess DNA integrity in control and iron-treated H9c2 cells, near full-length mtDNA amplification was performed using a GeneAmp XL PCR kit (PerkinElmer Life Sciences). The reaction mixtures contained 20 ng of total cellular DNA as a template, 0.4 µM of each primer, 1.2 mM magnesium, and 0.5 unit of recombinant *Thermus thermophilus* DNA polymerase in a total volume of 25 µl. Primers for amplification of the 15.9-kb fragment of mtDNA were 5'-CCT CCC ATT CAT TAT CGC CGC CCT TGC-3 (sense) and 5'-GAT GGG GCC GGT AGG TCG ATA AAG GAG-3 (antisense). To produce a 200-bp fragment of mtDNA (as a control for mtDNA input) the primers were 5'-CCT CCC ATT CAT TAT CGC CGC CCT TGC-3' (sense) and 5'-GTC TGG GTC TCC TAG TAG GTC TGG GAA-3' (antisense) (13). The near full-length mtDNA PCR was initiated at 75 °C for 3 min followed by 1 min at 94 °C and 25 cycles of 94 °C for 15 s, 68 °C for 12 min and final extension at 72 °C for 15 min. The 200-bp PCR was started at 95 °C for 2 min then 25 cycles of 95 °C for 1 min, 55 °C for 1 min, 72 °C for 1 min, and final extension at 72 °C for 5 min

(14). The amplified products were resolved on 0.8% agarose gels (15.9 kb) and 1.2% agarose gels (200 bp) containing 0.5% ethidium bromide. The PCR products were quantified with PicoGreen using a plate reading spectrofluorometer at 485 nm excitation and 525 nm emission.

To determine whether iron-mediated DNA damage was specific for mtDNA or perhaps shared by nuclear DNA, we also performed PCR amplification of a long fragment of the nuclear transferrin receptor gene (16.1 kb) as well as a short segment of the β-globin gene (265 bp). The reaction mixture contained 200 ng of total cellular DNA as a template, 0.4 μM of each primer, and 1.2 mM magnesium. Primers for amplification of the long fragment of the transferrin receptor gene (primer sequence from Occam Biolabs, Wilmington, DE) were 5'-GCA TAT TGG AAC ACT TGT GAG GGT GG-3'(sense) and 5'-AGA AGA CAT GCG CTT AGA TGC CAG AA-3' (antisense). For the 265-bp fragment of the β-globin gene (as a control for input of nuclear DNA) the primers were 5'-CCA ATC TGC TCA CAC AGG-3(sense) and 5'-CAC CTT TCC CCA CAG G-3' (antisense). The long length nuclear gene PCR was initiated at 75 °C for 3 min followed by 1 min at 94 °C and 25 cycles of 94 °C for 15 s, 68 °C for 12 min, and final extension at 72 °C for 15 min. The 265-bp β-globin fragment PCR was started at 95 °C for 2 min, then 25 cycles of 95 °C for 1 min, 55 °C for 1 min, 72 °C for 1 min, and final extension at 72 °C for 5 min. Amplified products were resolved and quantified as described above.

Quantitative Real-time Reverse Transcript (qRT)-PCR—Total RNA was extracted using an Rneasy® Mini Kit (Qiagen). Two μg of total RNA was converted to cDNA with Moloney murine leukemia virus reverse transcriptase and random primers $p(dN)_6$ (Promega, Madison, WI). qRT-PCR was performed using the Power SYBR® Green PCR Master Mix (AB Applied Biosystems, Foster, CA) on the DNA Engine Opticon real-time system (Bio-Rad). qRT-PCR was done for mRNAs encoded by both nuclear and mitochondrial genes. Nuclear genes were: iso-1-cytochrome *c* (*Cyc1*), succinate dehydrogenase subunit b (*Sdh* subunit b), cytochrome *c* oxidase Vb (*Cox vb*), nuclear respiratory factor 1 (*Nrf1*), and glyceraldehyde-3-phosphate dehydrogenase. Mitochondrial genes were: 16 S rRNA, NADH dehydrogenase subunit 4 (*Nd4*), cytochrome *c* oxidase subunit 1 (*Cox1*), and NADH dehydrogenase subunit 1 (*Nd1*). The primers used are listed in supplementary data Table S1. The thermal cycler conditions were as follows: 10 min at 95 °C followed by 40 cycles of 95 °C for 15 s and 60 °C for 1 min. Finally the samples were held at 65 °C for 5 min and melting curves were performed from 65 to 95.1 °C. All tests were performed in triplicate and all experiments were repeated three times. The amplification data were analyzed with Opticon Monitor analysis software. Calculations were based on the "Delta-Delta method" using the equation: R (ratio) = $2^{-[\triangle CT\ sample\ -\triangle CT\ control]}$ (15). The integrity of amplified DNA was confirmed by determination of melting temperature. The data were expressed as -fold changes of the treatment groups in relation to the controls.

Mitochondrial DNA Isolation and 8-Oxo-deoxyguanosine (8-Oxo-dG) Quantification—Mitochondrial DNA was isolated from control and iron-treated H9c2 cells with the *BioVision* mitochondrial DNA isolation kit (BioVision, Mountain View, CA). Prior to DNA isolation,

the intact mitochondria were digested with DNase (Promega, Madison, WI) to prevent nuclear DNA contamination (which was checked by PCR amplification of a 256-bp segment of the β-globin gene). The purity of the isolated mitochondria was estimated by measurements of acid phosphatase activity (because impure preparations are most likely to be contaminated by lysosomes). As expected, acid phosphatase activity of whole cell lysates was quite high but the enzyme activity was undetectable in isolated mitochondria (*i.e.* <0.1% of whole cell activity/mg of protein).

Following mtDNA isolation, 8-oxo-dG adducts were measured using a commercial enzyme-linked immunosorbent assay kit (Trevigen Inc., Gaithersburg, MD). Briefly, 1 μg of mtDNA was combined with anti-8-oxo-dG antibody and the samples were incubated overnight at 4 °C. Twenty-four hours later, the samples were added to 96-well microtiter plates containing bound albumin:8-oxo-dG adducts and incubated at room temperature for 2 h. The plate was then washed and incubated with a peroxidase-coupled secondary antibody at room temperature for 1 h in the dark. The plate was then washed (6 times) and tetramethylbenzidene substrate was added to each well and incubated for 15 min in the dark. After the addition of a stop solution, absorbance was read at 450 nm. Results were calculated based on a standard curve run simultaneously.

Establishment of H9c2 rho^{o} Cells—H9c2 cells were cultured under otherwise standard conditions in DMEM supplemented with 4 mg/ml glucose, 100 μg/ml pyruvate, and 50 μg/ml uridine to compensate for (i) respiratory incompetence, (ii) pyridine nucleotide redox imbalance, and (iii) pyrimidine/purine auxotrophy, respectively, arising from mitochondrial dysfunction. Ethidium bromide (1 μg/ml) and chloramphenicol (50 μg/ml) were added and the cells were cultured under these conditions for 10 months at which time testing of mitochondrial membrane potential with JC-1 indicated that most of the cells were rho^{o}. For estimation of mitochondrial membrane potential, JC-1 was added to the cell culture for 30 min at 37 °C at a final concentration of 5 μM. The cells were then washed three times in HBSS (containing Ca^{2+} and Mg^{2+}) and examined by fluorescence microscopy.

The cells were subcloned by limiting dilution and the clones were maintained in the same supplemented culture medium (above) for four passages. At that point, the rho^{o} status of individual clones was verified by (i) absence of JC-1 staining (mitochondrial membrane potential), (ii) absence of the 200-bp PCR product for mtDNA, (iii) lack of cytochrome *c* oxidase activity (measured as described below), and (iv) failure to grow in non-supplemented DMEM.

Estimation of ROS Production by Iron-loaded Cardiac Myocytes—ROS production was assessed by following the oxidation of DCF-DA. H9c2 cells and rho^{o} H9c2 cells were plated onto 48-well plates at an initial density of 2 x 10^4 cells per well in supplemented DMEM. When the cells were >60% confluent (second or third day) 300 μM FAC was added. After 24 h in culture, the cells were washed three times with HBSS (containing Ca^{2+} and Mg^{2+}). ROS production was estimated following the addition of 10 μM DCF-DA (final concentration) and DCF fluorescence was followed for 1 h using a thermostated plate reading spectrofluorometer

(520 nm excitation and 610 nm emission). Relative fluorescence was corrected for variations in cell protein between individual wells.

Oxygen Consumption Measurements—H9c2 cells were cultured on 150-cm plates. When the cells reached 60% confluence, 300 μM FAC was added. Following 7–11 days, the cells were washed once with PBS, detached with trypsin-EDTA, and suspended in complete culture medium. The cells were concentrated by centrifugation at 2,000 x *g* for 10 min and resuspended in culture medium. Respiration was measured with and without the addition of 20 μM CCCP (an uncoupler) using a Gilson Oxygraph with a Clark electrode (Yellow Springs Instrument Co., Yellow Springs, OH). Respiration rates were measured using 5 x 10^6 cells suspended in a total volume of 3.0 ml of DMEM containing 10% fetal bovine serum and supplemented with 17 mM glutamate at 37 °C. A starting O_2 concentration of 240 μM was assumed based on O_2 solubility at sea level at 37 °C. Results were adjusted for variations in the numbers of viable cells as determined by trypan blue exclusion.

Cytochrome c Oxidase Assay—H9c2 cells were detached from the culture flask as above, washed twice with ice-cold PBS, and counted. After centrifugation at 1000 x *g* for 8 min, the cell pellets were disrupted ultrasonically using 3 x 1-s bursts from a microtip oscillator (Fisher Scientific) in lysis buffer (20 mM Tris, pH 7.5, 1 mg/ml BSA, 50 mM KCl, 0.25 M sucrose, 0.5% Tween 80, 2 mM EDTA). The lysate was centrifuged at 4000 x *g* for 10 min. The pellet was discarded and the supernatant was used for the assays (16). The assays contained ~30 μg of protein and were performed in a 200-μl reaction volume. The assay involved the addition of 40 μM reduced cytochrome *c* in an isoosmotic medium (20 mM KH_2PO_4, pH 6.5, 100 mM KCl, 1 mg/ml BSA, 0.3 M sucrose) containing 2.5 mM *n*-dodecylmaltoside to permeabilize mitochondrial membranes. The activity was calculated from the rate of decrease in absorbance of ferrocytochrome *c* at 550 nm (absorbance coefficient = 19.1 mM^{-1} cm^{-1}) (17) and results were normalized by protein.

NADH Dehydrogenase Assay—This enzyme activity was measured as described by Boffoli *et al*. (18). The reaction employed 40 μM ferricytochrome *c* and 200 μM NADH in 25 mM potassium phosphate, 5 mM $MgCl_2$, 10 mM Tris (pH 8.0) buffer containing 1 mg/ml BSA, 0.24 mM KCN, and 0.4 μM antimycin A. Activity was followed spectrophotometrically for a total of 5 min at 550 nm, read every 15 s for 120 cycles, using a Biotek plate reader (BioTek, Winooski VT). Activity was calculated from the reduction of cytochrome *c* at 550 nm (using an absorbance coefficient of 19.1 mM^{-1} cm^{-1}) and expressed per mg of protein (16, 19).

Citrate Synthase Assay—This assay was performed as described by Williams *et al.* (20) with minor modifications. It is based on the reaction of oxaloacetate and acetyl-CoA to produce *coenzyme A*, the latter being detected by 5,5'-dithiobis(2-nitrobenzoic acid), which reacts with sulfhydryls in coenzyme A producing thionitrobenzoate. The assay mixture contained, in a total volume of 200 μl, 10 μl of cell extract, 2 mM 5,5'-dithiobis(2-nitrobenzoic acid), 0.1 mM acetyl-CoA, and 12 mM oxaloacetic acid in 10 mM KH_2PO_4 (pH 7.8) containing 2 mM EDTA, 1 mg/ml BSA, and 0.1% Triton X-100. The formation of thionitrobenzoate was

followed at 412 nm for 30 min and results were expressed as nanomole/min/mg of protein using an absorbance coefficient of 13.6 mM^{-1} cm^{-1} (21).

Results

Cytotoxic Effects of Iron

Following 4 days exposure to 300 μM iron (added as FAC), H9c2 cells showed diminished growth and increased cytotoxicity (Fig. 1). These cytostatic and cytocidal effects of iron were accompanied by an accumulation of intracellular, cytosolic iron. When H9c2 cells were cultured in the presence of a non-cytotoxic dose of 200 μM iron for 24 h, the presence of intracellular iron was easily detected using calcein fluorescence (Fig. 2). When calcein binds iron, this normally fluorescent compound is quenched and gives a visual approximation of the amounts of free (*i.e.* chelatable) intracellular iron. Note that the punctate fluorescence in Fig. 2*B* probably arises from the acidic lysosomal compartment. At lysosomal pH (~4.5) iron (which is normally abundant in lysosomes) will not quench calcein fluorescence. The amounts of iron accumulated by cells exposed to 300 μM iron over time are shown in Table 1. The increased intracellular concentration of free (presumably redox active) iron may be particularly important. We should note that determinations of total intracellular iron in rho^o H9c2 cells exposed to 300 μM FAC for 6 days showed similar iron accumulation (29.4 ± 1.6 $nM/10^6$ cells).

TABLE 1: Iron uptake by H9c2 cells

H9c2 cells were cultured for 3–6 days in the presence of 300 μM FAC. Following exposure to iron, the cells were detached with trypsin/EDTA containing 1 mM desferrioxamine equivalents of the high molecular weight hydroxyethyl starch: desferrioxamine conjugate to remove any extracellular iron and iron content was measured as described under "Experimental Procedures." n = 3 in all cases.

Treatment with iron	Free iron	Protein bound iron	Total iron
		nmol/million cells	
Untreated	0.58 (±0.062)	2.12 (±0.29)	2.70
3 days, 300 μM	1.34 (±0.014)[a]	15.43 (±0.98)[a]	16.76
6 days, 300 μM	1.67 (±0.089)[a]	26.08 (±0.98)[a]	27.75

[a] $p < 0.05$ for control *versus* iron exposed cells (Student's *t* test, two-tailed).

Iron Loading Leads to Protein Carbonyl Accumulation

One measure of the extent of metal-catalyzed oxidation events is the accumulation of protein carbonyls, predominantly glutamic and aminoadipic semialdehydes (22). Measurement of protein carbonyls following 7 days of culture in the presence of 300 μM FAC showed that substantial oxidation occurred in mitochondrial proteins (control cells = 0.47 ± 0.1, iron-treated cells = 2.9 ± 0.47 nmol of carbonyls/mg of protein; $n = 3$, $p < 0.01$). In contrast, total cellular protein carbonyls were lower and increased less upon iron loading (control cells = 0.23 ± 0.03, iron-treated cells = 0.43 ± 0.07 nmol carbonyls/mg protein; $n = 3$) suggesting that iron-driven protein oxidation preferentially affects mitochondria (23).

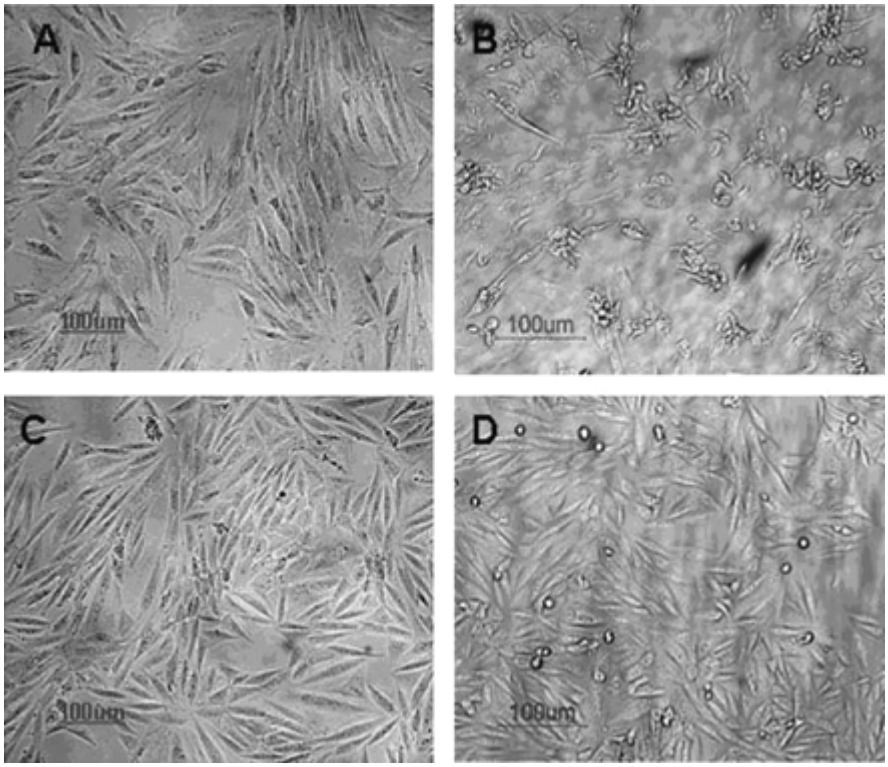

FIGURE 1: Morphology of cardiac myocyte H9c2 cells and H9c2-rho^o cells were grown in the absence or presence of 300 μM FAC. A, control H9c2 cells. B, H9c2 cells grown in the presence of 300 μM FAC for 4 days. C, control H9c2 rho^o cells grown in the absence of 300 μM FAC. D, H9c2 rho^o cells grown in the presence of 300 μM FAC for 4 days. Note that FAC appears to be preferentially toxic to the wild-type H9c2 cells versus the rho^o cells.

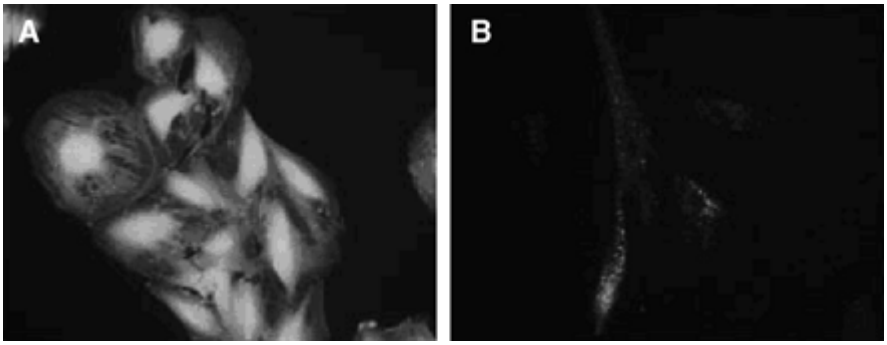

FIGURE 2: Calcein staining of H9c2 cells grown in the absence (A) or presence (B) of 200 μM FAC for 24 h. Substantial intracellular iron was present following iron exposure as shown by the quenching of calcein fluorescence (B).

Chronic Iron Exposure Leads to Mitochondrial DNA Damage
Accumulation of 8-Hydroxy-2'-deoxyguanosine—As shown in Fig. 3, cells exposed to 300 μM FAC for 3 and 7 days showed 3- and 7-fold increases in 8-oxo-dG in mtDNA. Such a progressive increase might be expected to result from exposure to increased iron. However, we should emphasize that the accumulation of 8-oxo-dG would not explain the loss of full-length PCR amplifiable mtDNA described below because 8-oxo-dG causes only minor slowing of polymerase replication (24).

Loss of Full-length mtDNA—The use of long range PCR to estimate the integrity of mtDNA is based on the principle that several types of DNA damage, such as single or double strand breaks or bulky base modifications, will block the polymerase, leading to decreased total PCR product (13, 14). We found that H9c2 cells exposed to 300 μM iron for 7 and 14 days showed a substantial reduction in the amount of 15.9-kb mtDNA product (Fig. 4*A*), whereas no changes were found in the PCR product of a similar length of nuclear DNA (Fig. 4*B*). This was true whether the amount of product was expressed relative to that of non-iron-exposed cells or as a ratio of long range product *versus* the 200–265-bp products from the same cells. Amounts of the latter products were virtually unaffected by iron loading of cells. As shown in Fig. 5, the majority of this loss of full-length mtDNA occurs during the first 3–4 days of iron exposure. We should note that this particular assay only indicates the *presence* of mtDNA damage but not the *extent* of such damage inasmuch as diminished long product formation could arise from only a single break or modification (or, for that matter, could reflect more extensive damage).

H9c2-rho^{o} Cells Have a Survival and Growth Advantage during Iron Overload
Because iron-mediated cellular damage requires cellular oxidizing and reducing equivalents, we tested the effects of iron excess on rho^{o} H9c2 cells, the mitochondria of which generate little or no ROS. These cells were highly resistant to the toxic effects of elevated iron compared with wild-type H9c2 cells. Fig. 6 shows changes in cell numbers during 4 days growth in the presence and absence of added iron. (Note that as a consequence of their rho^{o} status these cells grow at a substantially slower rate than do the wild-type H9c2 cardiac myocytes.) Similar results after 4 days iron exposure were obtained using measurements of Alamar blue reduction (which is unaffected by rho^{o} status; data not shown). After even short

term iron exposure, we found increases in ROS generation but only in the wild-type H9c2 cells (Fig. 7).

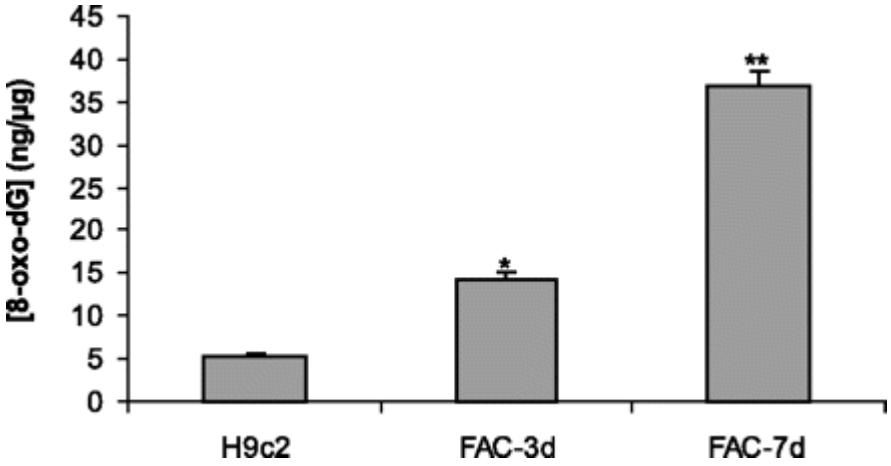

*FIGURE 3: 8-Oxo-dG accumulation in purified mtDNA measured by enzyme-linked immunosorbent assay in H9c2 cells before and 3–7 days after exposure to 300 µM FAC. Results are expressed as nanograms of 8-oxo-dG/mg of total mtDNA ± 1 S.D. differ from control cells not exposed to iron. *, $p < 0.05$; **, $p \leq 0.001$ (Student's t test, two tailed). n = 3 separate preparations in each case.*

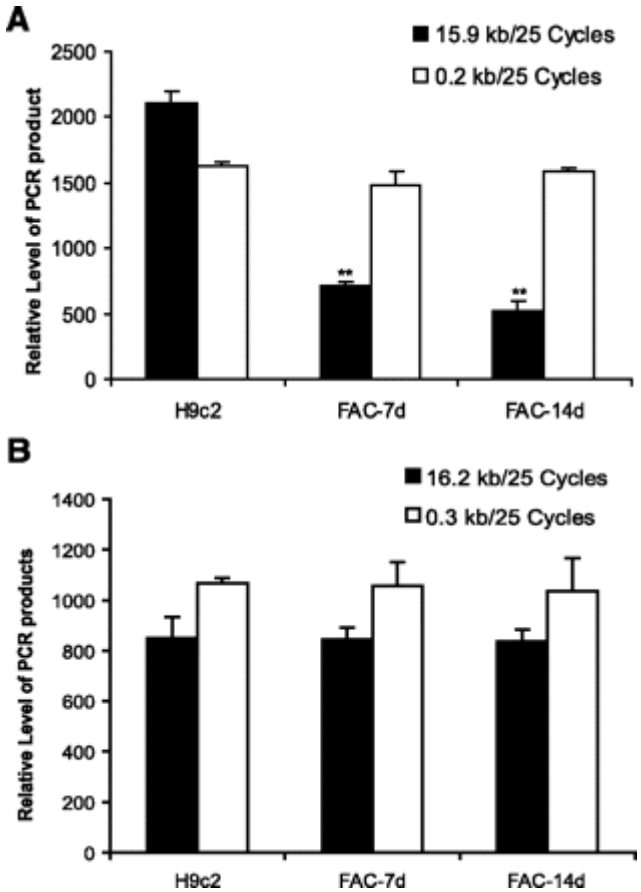

FIGURE 4: Iron loading causes progressive loss of near full-length (PCR-amplifiable) mtDNA. H9c2 cells were exposed 300 µM iron for 7 and 14 days. The total DNA was isolated that was amplified with qPCR. Full-length mtDNA product was significantly decreased after 7 and 14 days (A), whereas no changes were observed in the PCR product of an equally long segment of the transferrin receptor nuclear gene (B). $p < 0.01$ for mitochondrial versus nuclear long length products (Student's t test, two-tailed). n = 3 separate preparations in each case.

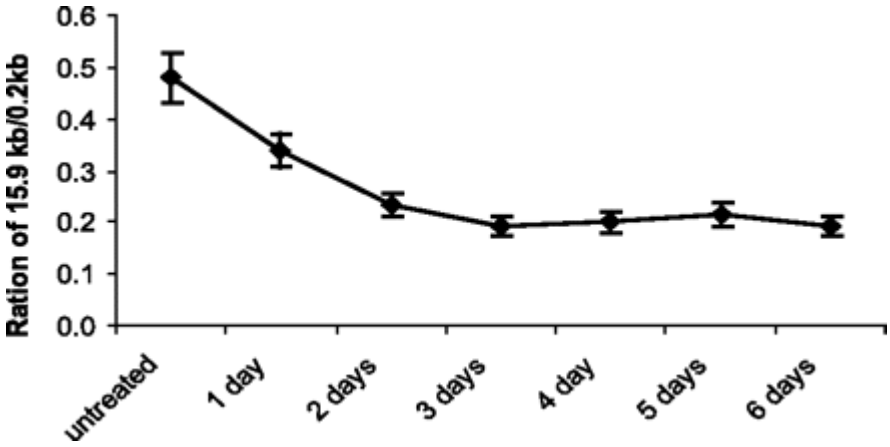

FIGURE 5: Progressive loss of full-length (PCR-amplifiable) mtDNA during exposure of cultured H9c2 cells to 300µM FAC. Results shown are the mean ± 1 S.D. of the ratio of near full-length versus 200-bp amplification products. All values differ significantly from untreated controls at $p < 0.05$ (Student's t test, two-tailed). n = 4 separate preparations for each point.

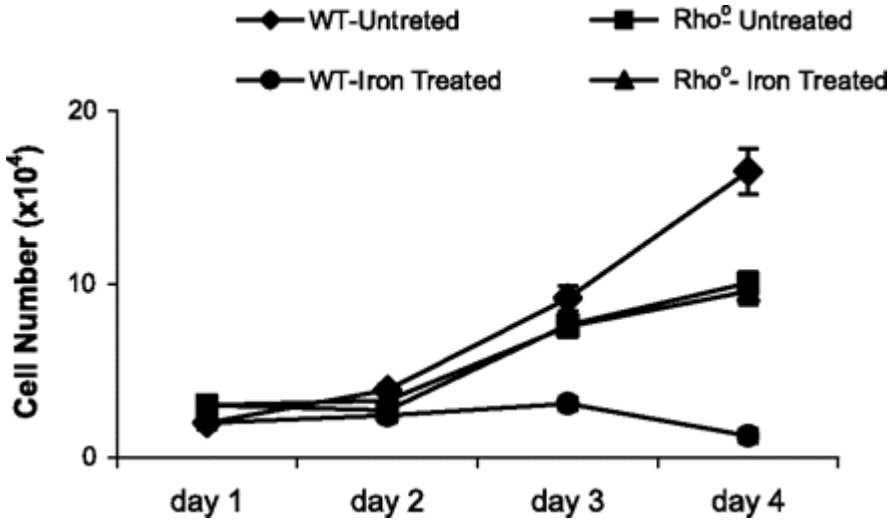

FIGURE 6: Growth of wild-type and rho^o H9c2 cells in the absence and presence of iron. Control and rho^o H9c2 cells were cultured for up to 4 days in normal medium or medium containing 300 µM FAC. At each time point, trypan blue excluding cells were counted using a hemocymeter. Each point represents the mean of four independent assays ± 1 S.D. Iron-exposed rho^o H9c2 cells grew at the same rate as the control rho^o cells, whereas wild-type H9c2 cells exposed to iron grew very little over the first 3 days and then began dying. For iron-exposed wild-type versus rho^o cells exposed to iron, cell numbers differ significantly on days 3 and 4 at $p < 0.001$ (n = 4 in all cases).

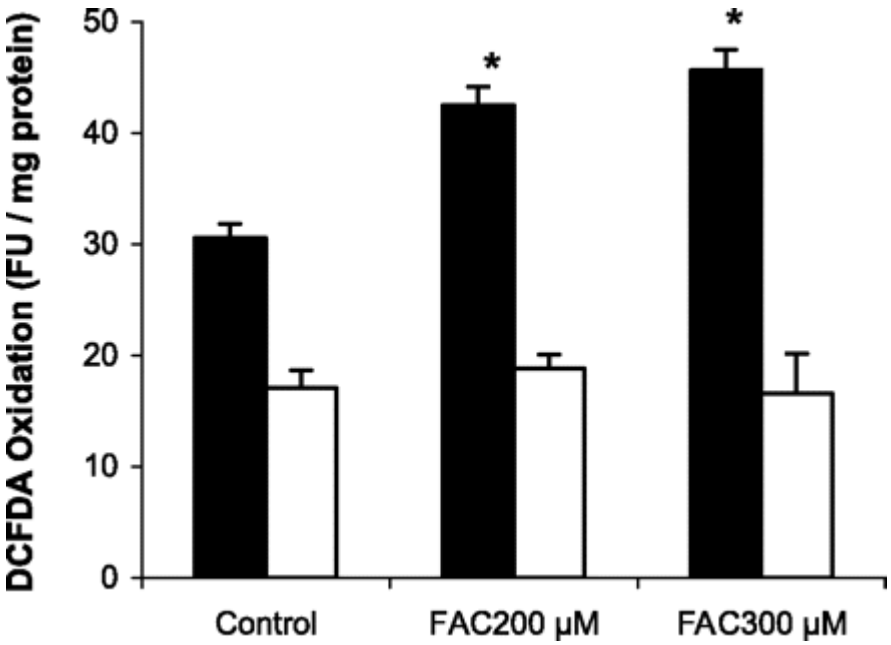

FIGURE 7: Iron-induced ROS generation in wild-type and rho^o H9c2 cells. ROS production was examined after 24 h of culture in the absence or presence of 200 and 300 µM iron using oxidation of the fluorescent probe DCF-DA. Whereas ROS production in wild-type H9c2 cells (filled bars) was significantly increased by iron exposure, no changes were observed in rho^o H9c2 cells (open bars). $p < 0.05$ for rho^o versus wild type cells (Student's t test, two-tailed). $n = 4$ in all cases.

Mitochondrial DNA Damage Is Associated with Decreases in the Activity of Respiratory Chain Components and Diminished Respiratory Function

In view of the cumulative iron-mediated damage to mtDNA, we examined the effects of iron exposure on the respiration of H9c2 cells. Long-term exposure to elevated iron in the culture medium caused H9c2 cells to progressively lose respiratory capacity. Cells exposed to 300 µM iron for up to 11 days showed almost 60% reduction in uncoupled oxygen consumption (*i.e.* in the presence of CCCP) (Fig. 8*A*) and in the absence of an uncoupler (Fig. 8*B*). Note that these results were corrected for numbers of viable (*i.e.* trypan blue excluding) cells.

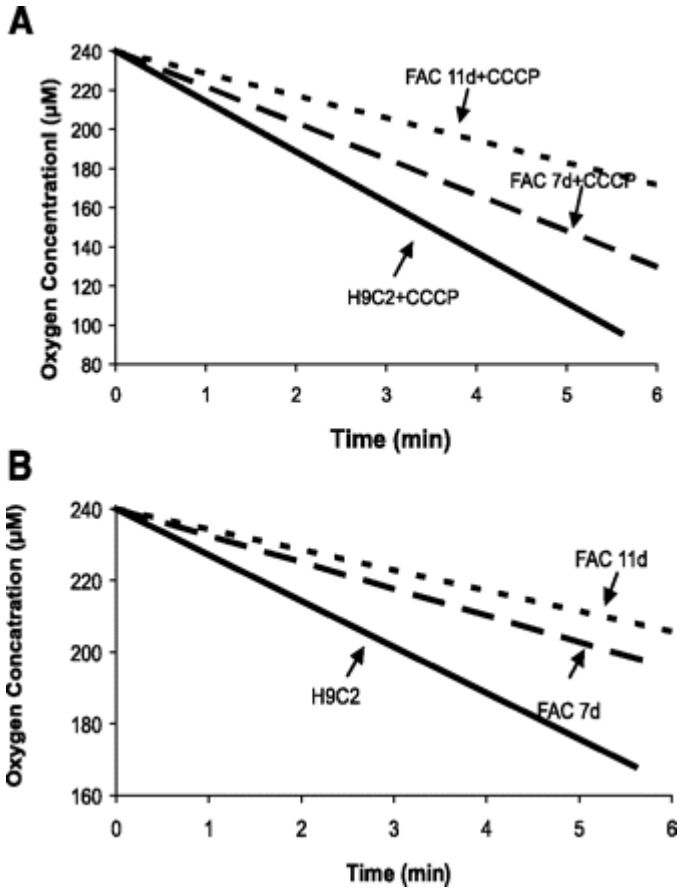

FIGURE 8: Decreased oxygen consumption by H9c2 cells exposed to 300 µM iron for 7 or 11 days. Respiration rates were measured using 3–5 x 10^6 viable cells (determined by trypan blue exclusion) and results were adjusted mathematically to rate of oxygen consumption per 5 x 10^6 viable cells. A starting O_2 concentration of 240 µM was assumed based on O_2 solubility at sea level at 37 °C. Compared with untreated H9c2 cells, maximal oxygen consumption rates in the presence of the uncoupler CCCP were significantly decreased following iron exposure at both 7 and 11 days (A). Similar iron-mediated decrements in respiration were also observed in the absence of an uncoupler (B). $p < 0.01$ untreated versus iron-treated cells (Student's t test, two-tailed). n = 3 separate cell preparations in each case.

The decreased oxygen consumption was accompanied by decrements in the activities of both complexes I and IV (Table 2). Diminished activity of these respiratory chain components may reflect decreased transcription of mRNA specifically for subunits encoded by mtDNA. Thus, as shown in Fig. 9, qRT-PCR products for three mitochondrially encoded respiratory chain components and mitochondrial 16 S rRNA were substantially lower in iron-exposed H9c2 cells, whereas products for four nuclear-encoded subunits remained at or above control levels. This implies a preferential decrease in mitochondrial *versus* nuclear mRNA species, likely reflecting the extensive iron-mediated damage to mtDNA.

TABLE 2: Changes in cytochrome c oxidase (COX) and NADH dehydrogenase activities (both having subunits encoded by the mitochondrial genome) versus citrate synthase (nuclear encoded) in H9c2 cells exposed to iron for 3 and 7 days

Data shown are mean ± 1 S.D. of three independent cultures.

Cell line/treatment	Citrate synthase	Cytochrome *c* oxidase activity	Ratio of COX/citrate synthase	NADH dehydrogenase activity	Ratio of NADH/citrate synthase
	nmol/min/mg protein			*nmol/min/mg protein*	
Untreated	4.39 ± 0.36	8.75 ± 0.52	1.99 ± 0.44	1.37 ± 0.06	0.64 ± 0.42
FAC300-3 days	6.14 ± 0.37	6.25 ± 0.76[a]	1.02 ± 0.56[a]	0.53 ± 0.04[a]	0.32 ± 0.21[a]
FAC300-7 days	4.35 ± 0.11	5.27 ± 0.15[a]	1.21 ± 0.28[a]	0.47 ± 0.01[a]	0.40 ± 0.06[a]

[a] $p < 0.01$ *versus* untreated H9c2 cells (Student's *t* test, two-tailed).

Discussion

Damage to cells and organs caused by chronic iron overload affects a wide range of tissues. Especially in patients with secondary (transfusion-mediated) iron overload, heart failure is a prominent cause of death (25, 26). In this case, clinically important cardiac dysfunction often requires years to appear following the establishment of an iron overload state. It is highly likely that the pathologies caused by iron overload involve iron-driven oxidation reactions, but the slow onset implies some kind of biological "memory" through which the cumulative damage is ultimately translated into organ failure.

The present work represents an attempt to determine whether cellular iron overload might cause cumulative damage to mtDNA and, if so, whether such damage might eventuate in mitochondrial dysfunction. Mitochondrial DNA is especially vulnerable to oxidative damage and has less efficient repair systems for some kinds of damage (27). Furthermore, mtDNA resides within the organelle that generates most of the ROS produced by cells such as cardiac myocytes. It was shown many years ago that oxidant-induced damage to naked DNA and intracellular DNA is greatly enhanced by iron (28, 29) and, in the absence of transition metals (such as iron and copper), DNA is quite unreactive with oxidants such as H_2O_2. The products of iron-mediated DNA damage are not fully characterized but include strand breaks, oxidatively modified bases, DNA-protein cross-links (30, 31), covalent reactions with lipid peroxidation products (32), and other structurally uncharacterized bulky DNA adducts (33).

The relative importance of these modifications in long-term or irreversible oxidative DNA damage is not yet known.

In the present investigations we found that exposure of H9c2 cardiac myocytes to elevated iron concentrations leads to a progressive increase in 8-oxo-dG content of mtDNA and decrease in intact mtDNA as judged by loss of near full-length PCR-amplifiable mtDNA. This loss appears to be restricted to mtDNA inasmuch as PCR amplification of an equally long segment of a nuclear gene for the transferrin receptor shows little or no iron-induced change in the amount of product.

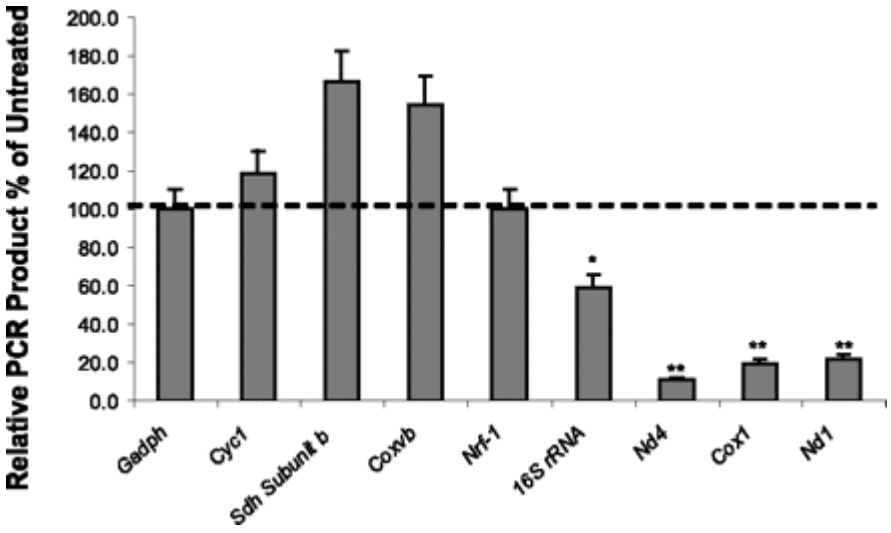

*FIGURE 9: Decreased mRNA for respiratory chain components (and 16 S rRNA) following iron exposure of H9c2 cells. H9c2 cells were exposed to 300 µM iron for 7 days. Real-time PCR was used to detect levels of mRNA expression of mitochondrial genes (16 S rRNA, Nd4, Cox1, and NdI) and nuclear genes (GADPH, Cyc1, Sdh subunit b, Cox vb, and Nrf1). Results suggest 50–90% loss of mRNAs encoded by mtDNA but no decreases in those encoded by nuclear genes. Gapdh mRNA was used as an input control. **, $p < 0.001$ untreated versus iron-treated H9c2 cells (Student's t test, two-tailed). $n = 3$ in each case.*

Although the observed damage to mtDNA caused by iron exposure increases with time of exposure, the changes seem to occur over the first few days (whereas the damage that may occur in iron-overloaded humans clearly takes much longer). It is difficult, however, to extrapolate from results with cultured cells to time-dependent changes in humans. First, the amounts of iron to which the cultured cells are exposed are probably higher than the level of non-transferrin bound iron in patients with iron overload. Second, the pro-oxidant effects of iron load may be magnified in the cultured cardiac myocytes by the unphysiologically high oxygen concentration in culture (>120 mmHg) *versus in vivo* (<20 mm Hg). Third, the amounts of intracellular iron may be exaggerated in the cultured cells exposed to exogenous iron. However, with regard to the latter point, we find an ~10-fold increase in intracellular iron after 6 days exposure to 300 µM FAC, a value in line with the estimated cardiac iron load in the gerbil model of iron cardiomyopathy and by extrapolation from magnetic resonance T2* (the iron-sensitive relaxation time) in humans (34).

Associated with this progressive loss of "intact" mtDNA, there was a parallel decline in mitochondrial respiration (Fig. 8). This respiratory dysfunction probably arises from defective synthesis of respiratory chain subunits encoded by mtDNA but may also reflect oxidative damage to mitochondrial proteins. Using qRT-PCR we observed decreased amounts of mRNAs encoded by four mitochondrial genes, whereas the levels of mRNAs for four respiratory chain subunits encoded by nuclear DNA were unaffected by long-term iron exposure.

Iron-mediated damage to mtDNA likely involves the conspiracy of mitochondrially generated ROS. The mitochondrial electron transport chain leaks 1–2% of its electrons into O^{-}_{2}/H_2O_2 (35) (although more recent work (36, 37) suggests lower estimates). This is the primary source of the ROS generated by most cell types. The importance of mitochondrially generated ROS in cellular iron toxicity is emphasized by our finding that rho^{o} H9c2 cells (which produce very little detectable ROS) are relatively immune to the cytostatic and cytotoxic effects of iron overload.

We should re-emphasize that the model used for these investigations, relatively short term exposure of a cultured cardiac myocyte cell line to relatively high concentrations of iron, probably does not adequately reflect the changes that might occur in the hearts of humans with chronic iron overload. However, the results do suggest aspects of the latter (especially the relative expression of mitochondrially encoded respiratory chain subunits and the integrity of mtDNA), which might now be investigated. Furthermore, our results do not mean that iron-mediated damage to mtDNA is a full explanation of the cell and organ damage caused by increased iron. In this regard, iron-mediated destabilization of lysosomal membranes represents an alternative, perhaps additive, mechanism of damage arising from iron within the cellular lysosomal compartment. Intralysosomal iron sensitizes lysosomes to damage by endogenous oxidants such as H_2O_2. The resultant destabilization of the lysosomal membrane can lead to the release of damaging lysosomal digestive enzymes and iron into the cytoplasm of the cell (38–40). The potential importance of lysosomal instability in the specific case of iron overload has been suggested by others (41) and iron-mediated lysosomal instability and enhanced lipid peroxidation do occur in animal models of iron overload (42). In fact, Stal and colleagues (43) suggest that the changes in hepatic lysosomal volume density in idiopathic hemochromatosis correlate very well with the extent of iron overload and are effectively reversed upon iron removal. However, it is not established whether, *in vivo*, these lysosomal abnormalities are an important pathophysiologic factor.

Overall, our results support the idea that long-term iron-mediated damage to cells and organs is associated with progressive damage to mtDNA. This can lead to decreased synthesis of respiratory chain subunits encoded by the mitochondrial genome and subsequent loss of normal cellular respiration. This pathogenic mechanism suggests the possibility of a feed-forward mechanism in which mitochondria with sufficiently damaged genomes may become factories for the production of increased amounts of reactive oxygen species that, in turn, further accelerate organ damage. Finally, we should note that there are interesting parallels between the iron-mediated mitochondrial damage we have observed and the mitochondrial

damage found in patients with neurodegenerative diseases. Damage to mtDNA has been reported in a variety of such disorders (including Parkinson, Alzheimer, and Huntington diseases) (44). It is possible that progressive loss of mtDNA and associated metabolic changes may be important in these disorders as well.

References

1. Quinlan, G. J., Evans, T. W., and Gutteridge, J. M. (2002) *Free Radic. Biol. Med.* **33,** 1306–1313

2. Graf, E., Mahoney, J. R., Bryant, R. G., and Eaton, J. W. (1984) *J. Biol. Chem.* **259,** 3620–3624

3. Luo, Y., Han, Z., Chin, S. M., and Linn, S. (1994) *Proc. Natl. Acad. Sci. U. S. A.* **91,** 12438–12442

4. Loschen, G., Azzi, A., Richter, C., and Flohe, L. (1974) *FEBS Lett.* **42,** 68–72

5. Ryan, T. P., and Aust, S. D. (1992) *Crit. Rev. Toxicol.* **22,** 119–141

6. Yaffee, M., Walter, P., Richter, C., and Muller, M. (1996) *Proc. Natl. Acad. Sci. U. S. A.* **93,** 5341–5346

7. Ahmed, S. A., Gogal, R. M., Jr., and Walsh, J. E. (1994) *J. Immunol. Methods* **170,** 211–224

8. Qian, M. W., and Eaton, J. W. (1989) *Arch. Biochem. Biophys.* **275,** 280–288

9. Eskelinen, S., Haikonen, M., and Raisanen, S. (1983) *Scand. J. Clin. Lab. Investig.* **43,** 453–455

10. Artiss, J. D., Vinogradov, S., and Zak, B. (1981) *Clin. Biochem.* **14,** 311–315

11. Fuller, K. M., Duffy, C. F., and Arriaga, E. A. (2002) *Electrophoresis* **23,** 1571–1576

12. Levine, R. L., Garland, D., Oliver, C. N., Amici, A., Climent, I., Lenz, A. G., Ahn, B. W., Shaltiel, S., and Stadtman, E. R. (1990) *Methods Enzymol.* **186,** 464–478

13. Ayala-Torres, S., Chen, Y., Svoboda, T., Rosenblatt, J., and Van Houten, B. (2000) *Methods* **22,** 135–147

14. Yakes, F. M., and Van Houten, B. (1997) *Proc. Natl. Acad. Sci. U. S. A.* **94,** 514–519

15. Livak, K. J., and Schmittgen, T. D. (2001) *Methods* **25,** 402–408

16. Jarreta, D., Orus, J., Barrientos, A., Miro, O., Roig, E., Heras, M., Moraes, C. T., Cardellach, F., and Casademont, J. (2000) *Cardiovasc. Res.* **45,** 860–865

17. Kruidering, M., Van de Water, B., de Heer, E., Mulder, G. J., and Nagelkerke, J. F. (1997) *J. Pharmacol. Exp. Ther.* **280,** 638–649

18. Boffoli, D., Scacco, S. C., Vergari, R., Solarino, G., Santacroce, G., and Papa, S. (1994) *Biochim. Biophys. Acta* **1226,** 73–82

19. Bouaziz, N., Redon, M., Quere, L., Remacle, J., and Michiels, C. (2002) *Eur. J. Pharmacol.* **441,** 35–45

20. Williams, A. J., Coakley, J., and Christodoulou, J. (1998) *Anal. Biochem.* **259,** 176–180

21. Bejma, J., and Ji, L. L. (1999) *J. Appl. Physiol.* **87,** 465–470

22. Requena, J. R., Chao, C. C., Levine, R., and Stadtman, E. R. (2000) *Proc. Natl. Acad. Sci. U. S. A.* **98,** 69–74

23. Das, N., Levine, R. L., Orr, W. C., and Sohal, R. S. (2001) *Biochem. J.* **360,** 209–216

24. Tolentino, J. H., Burke, T. J., Mukhopadhyay, S., McGregor, W. G., and Basu, A. K. (2008) *Nucleic Acids Res.* **36,** 1300–1308

25. Aldouri, M. A., Wonke, B., Hoffbrand, A. V., Flynn, D. M., Ward, S. E., Agnew, J. E., and Hilson, A. J. (1990) *Acta Haematol.* **84,** 113–117

26. Gabutti, V., and Borgna-Pignatti, C. (1994) *Baillieres Clin. Haematol.* **7,** 919–940

27. Imam, S. Z., Karahalil, B., Hogue, B. A., Souza-Pinto, N. C., and Bohr, V. A. (2006) *Neurobiol. Aging* **27,** 1129–1136

28. Jackson, J. H., Schraufstatter, I. U., Hyslop, P. A., Vosbeck, K., Sauerheber, R., Weitzman, S. A., and Cochrane, C. G. (1987) *J. Clin. Investig.* **80,** 1090–1095

29. Schraufstatter, I., Hyslop, P. A., Jackson, J. H., and Cochrane, C. G. (1988) *J. Clin. Investig.* **82,** 1040–1050

30. Zastawny, T. H., Altman, S. A., Randers-Eichhorn, L., Madurawe, R., Lumpkin, J. A., Dizdaroglu, M., and Rao, G. (1995) *Free Radic. Biol. Med.* **18,** 1013–1022

31. Altman, S. A., Zastawny, T. H., Randers-Eichhorn, L., Cacciuttolo, M. A., Akman, S. A., Dizdaroglu, M., and Rao, G. (1995) *Free Radic. Biol. Med.* **19,** 897–902

32. Vaca, C. E., and Harms-Ringdahl, M. (1989) *Biochim. Biophys. Acta* **1001,** 35–43

33. Carmichael, P. L., Hewer, A., Osborne, M. R., Strain, A. J., and Phillips, D. H. (1995) *Mutat. Res.* **326,** 235–243

34. Wood, J. C., Otto-Duessel, M., Aguilar, M., Nick, H., Nelson, M. D., Coates, T. D., Pollack, H., and Moats, R. (2005) *Circulation* **112,** 535–543

35. Turrens, J. F., Alexandre, A., and Lehninger, A. L. (1985) *Arch. Biochem. Biophys.* **237,** 408–414

36. Hansford, R. G., Hogue, B. A., and Mildaziene, V. (1997) *J. Bioenerg. Biomembr.* **29,** 89–95

37. St. Pierre, J., Buckingham, J. A., Roebuck, S. J., and Brand, M. D. (2002) *J. Biol. Chem.* **277,** 44784–44790

38. Brunk, U. T., Neuzil, J., and Eaton, J. W. (2001) *Redox Rep.* **6,** 91–97

39. Persson, H. L., Yu, Z., Tirosh, O., Eaton, J. W., and Brunk, U. T. (2003) *Free Radic. Biol. Med.* **34,** 1295–1305

40. Yu, Z., Persson, H. L., Eaton, J. W., and Brunk, U. T. (2003) *Free Radic. Biol. Med.* **34,** 1243–1252

41. Link, G., Pinson, A., and Hershko, C. (1993) *J. Lab. Clin. Med.* **121,** 127–134

42. Peters, T. J., O'Connell, M. J., and Ward, R. J. (1986) in *Free Radicals and Liver Injury* (Poli, G., Cheeseman, K. H., Dianzani, M. U., and Slater, T. F., eds) pp. 107–115, IRL Press, Oxford

43. Stal, P., Glaumann, H., and Hultcrantz, R. (1990) *J. Hepatol.* **11,** 172–180

44. Yang, J.-L., Weissman, L., Bohr, V. A., and Mattson, M. P. (2008) *DNA Repair* **7,** 1110–1120